(Received 29 September 2025, Accepted 24 December 2025, Scheduled 10 January 2026)

Quantitative Comparison Study on the Impulse Characteristics of Typical Radial Grounding Electrodes in Transmission Lines

Wen Cao[1, *], Jiarui Zhang[1], Wei Shen[2], and Yasong Cao[1]

[1] *School of Electronic Information, Xi'an Polytechnic University, Xi'an 710048, China*
[2] *State Grid Shaanxi Electric Power Company Limited, Xi'an 710199, China*

ABSTRACT: To reveal the impulse behavior of radial grounding electrodes with different geometries, a comparative analysis was performed on three typical types: cross-shaped, Y-shaped, and rectangular ray-shaped electrodes. Existing research often examines only a single lightning waveform or influencing factor without addressing the coupled effects of the electrode shape and soil resistivity. In this work, CDEGS simulation software was used to analyze the lightning transient characteristics of the grounding electrodes. Multiple lightning current waveforms and soil resistivity levels were considered to quantitatively compare the power frequency resistance, impulse resistance, ground potential rise, step voltage, and frequency-domain response. The results indicated that the rectangular ray-shaped electrode exhibits better impulse performance in low-resistivity soils (150 $\Omega \cdot$ m), whereas the cross- and Y-shaped electrodes performed more effectively in high-resistivity soils (2000 $\Omega \cdot$ m). For mountainous regions with high lightning density, a cross-shaped configuration is preferred owing to its smaller footprint and lower inductive effect. In high-resistivity areas with infrequent lightning, a Y-shaped electrode provides a more favorable overall protection.

1. INTRODUCTION

With the advancement of industrialization and technological level, the global demand for electric power resources is increasing, thereby promoting the development of the electric power industry. As a critical channel of a power system, the safe operation of transmission lines is essential for maintaining system stability [1, 2]. Lightning is one of the primary causes of transmission line failure, and many countries experience a high proportion of outages caused by lightning strikes [3–5]. Lightning is a highly destructive natural phenomenon characterized by a high intensity, amplitude, and frequency. The spectral characteristics of the lightning current waveform also play a significant role in influencing the frequency-dependent behavior of the grounding impedance and the spatial distribution of transient fields in the soil [6–8]. As a key component of the tower lightning protection system, the grounding electrode is responsible for dissipating the lightning currents. A better impulse current dissipation performance results in a smaller tower-top potential rise, and thus, a higher lightning withstands the level of the transmission line [9–12]. Therefore, a rational design of grounding electrodes is crucial for improving lightning protection performance and ensuring the safe operation of transmission lines.

In the lightning protection design of tower grounding electrodes, studies on power-frequency grounding performance are relatively mature, and detailed specifications for the grounding resistance under various soil conditions have been established worldwide [13]. However, the research on the lightning impulse characteristics of grounding electrodes remains insufficient. Full-scale and scaled-model experiments can directly measure the impulse grounding resistance, but involve high costs and limited parameter adjustability [14–18]. With the advancement of computational technology, numerical simulations have become the primary approach for studying the lightning impulse characteristics of grounding electrodes. Compared with traditional experimental methods, simulations allow the precise construction of lightning current models and flexible adjustment of waveforms, amplitudes, soil parameters, and electrode geometries, enabling a more comprehensive evaluation of the grounding electrode behavior under impulse conditions. Based on numerical simulations, numerous studies have analyzed various factors and grounding electrode configurations. Nasir et al. [4] used CDEGS to model a rectangular ray-shaped electrode and investigated the influence of soil stratification on the impulse grounding resistance under a 10/350 µs lightning current. Bezerra et al. [19] examined the ground potential rise and pulse impedance of concrete-encased grounding electrodes while considering the frequency dependence of the soil parameters. Kumar et al. [20, 21] employed MATLAB-based dynamic circuit modeling to study the effects of lightning currents with different front times on vertical and horizontal enhancement electrodes, proposing an ECE expression and calculating the effective discharge length. Clark et al. [22] analyzed how the impulse grounding resistance varies with the vertical electrode length, lightning current amplitude, and horizontal electrode arrangement. Grcev et al. [23, 24] developed models for calculating the impulse grounding impedance of vertical, horizontal, and inclined electrodes, and validated them through numerical simulations. Xue et al. [25] combined field measurements with CDEGS modeling to study the effects of soil ion-

* Corresponding author: Wen Cao (caowen@xpu.edu.cn).

ization on tower grounding performance. Huang et al. [26] proposed a CFEM model suitable for the grounding electrode design in high-resistivity mountainous regions. Dan et al. [27, 28] introduced a new method for calculating the impulse grounding resistance and verified it using CDEGS. Gao et al. [29] used the ATP-EMTP (Electromagnetic Transients Program/Alternative Transients Program) to evaluate the effects of lightning current amplitude, electrode length, and conductor diameter. Qi and Zhao [30] and Shi et al. [31] utilized CDEGS to quantitatively compare the power-frequency and impulse characteristics of cross-, circular, and Y-shaped grounding electrodes.

Overall, most existing studies have focused on a single influencing factor, such as soil stratification or lightning current parameters, and lack a systematic investigation of the coupled effects between lightning characteristics and soil conditions. Furthermore, many studies have employed only one type of lightning waveform, which cannot capture the diversity of real lightning strikes. Because the impulse behavior of grounding electrodes is jointly governed by multiple factors, and the electrode geometry significantly affects the surface potential distribution, impulse potential rise, impulse grounding resistance, step voltage, and frequency-domain response, studies relying solely on a single waveform or a single metric are inadequate to fully characterize their physical behavior. To address the limitations of existing studies, this study developed a unified simulation framework and proposed a quantitative comparison method to systematically analyze the impulse characteristics of various radial grounding electrodes under different lightning current parameters and soil conditions. The aim is to provide physical insights and engineering guidance for selecting appropriate electrode geometries in different regions, thereby improving the overall lightning protection performance of the transmission lines.

In this study, models of cross-shaped, Y-shaped, and rectangular ray-shaped grounding electrodes were developed using the CDEGS simulation software, and the power frequency grounding resistance, impulse grounding resistance, ground potential distribution, step voltage potential distribution, and frequency domain response parameters of the three grounding electrodes were quantitatively compared under different lightning current waveforms and soil conditions. The aim is to provide a theoretical basis for the shape design of radial grounding electrodes in transmission lines under different soil conditions.

2. THEORETICAL CALCULATION METHODS

2.1. Power Frequency Grounding Resistance

Under idealized conditions, assuming that the grounding electrode has a specific geometric shape, the power frequency grounding resistance of various grounding electrodes can be derived using the electromagnetic field theory. For grounding electrodes with complex geometric shapes, numerical calculation methods for electromagnetic fields are employed, and regression analysis is used to fit the obtained numerical results to obtain the approximate value of the power frequency grounding resistance R_d. The specific calculation method is shown in (1) [32].

$$R_d = \frac{\rho}{2\pi L}\left(\ln\frac{L^2}{Dh} + A\right) \tag{1}$$

In (1): L is the total length of the grounding electrode; D is the diameter of the grounding electrode material (m); h is the burial depth of the grounding electrode (m); ρ is the soil resistivity of the area where the grounding electrode is laid; A is the shape factor of the grounding electrode distribution shape. According to the grounding code document DL/T621-1997, the shape factor for the rectangular ray-shaped grounding electrode is defined as $A = 1.76$, for the cross-shaped grounding electrode as $A = 0.89$, and for the Y-shaped grounding electrode as $A = 0$.

2.2. Impulse Grounding Resistance

The impulse grounding resistance R is a key parameter for assessing the lightning withstand level of transmission lines and can intuitively evaluate the operational safety of transmission lines. Unlike the calculation method of power-frequency grounding resistance R_d, the impulse grounding resistance R is defined as the ratio of the peak value U_m of the ground potential rise caused by the lightning current flowing through the grounding electrode into the earth to the amplitude I_m of the impulse current injected into the grounding electrode. The specific calculation method is shown in Equation (2).

$$R = \frac{U_m}{I_m} \tag{2}$$

2.3. Ground Potential Rise

When a transient lightning current flows through the grounding electrode into the soil, it causes an increase in the ground potential near the point of entry. The increase in ground potential is defined as V_s; the impulse factor is defined as k (the ratio of the impulse grounding resistance R to the power frequency grounding resistance R_d); I_m is the amplitude of the lightning current dissipated into the earth through the grounding electrode; and R_d is the power-frequency grounding resistance of the tower grounding electrode. The specific calculation method is given in (3) [32].

$$V_s = k \times I_m \times R_d \tag{3}$$

(3) employs theoretical calculation methods to analyze the ground potential rise parameters at the point of entry of the grounding electrode. However, this method struggles to intuitively display the overall distribution of the ground potential rise across the surface area caused by the grounding electrode under the influence of an impulse current. Because of the large number of surface calculation observation points and the fact that changes in the shape of the grounding electrode lead to differences in the distribution of the ground potential rise, solving the problem solely through theoretical calculations becomes complex. Therefore, it is necessary to use simulation methods to compare and analyze the surface ground potential rise distribution of grounding electrodes of different shapes under lightning strikes.

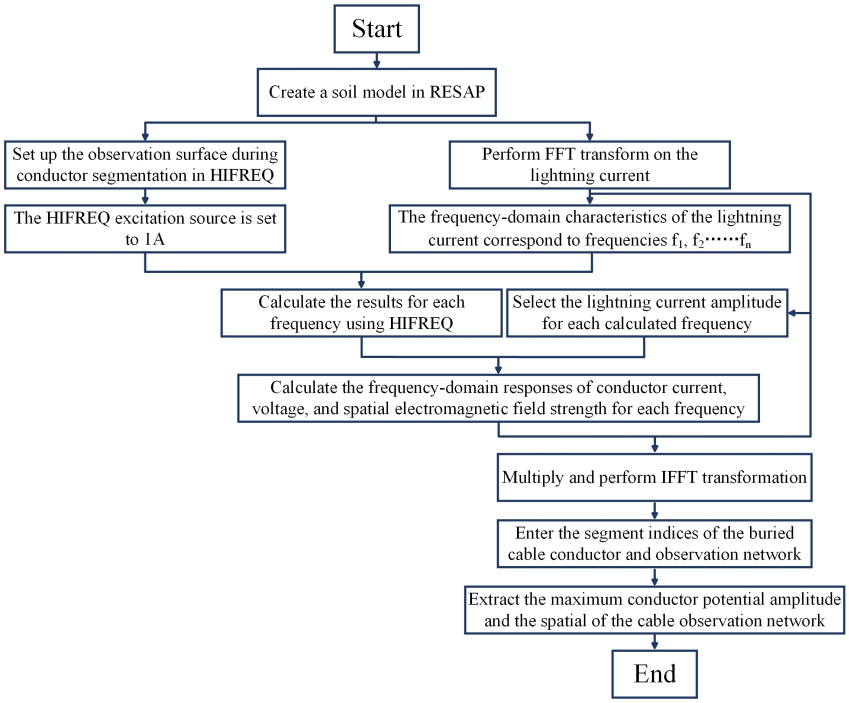

FIGURE 1. Internal principles of the simulation calculations.

2.4. Step Voltage

The GB50065-2011 and DL/T621-1997 code documents specify the safety limits of the step voltage under power frequency conditions for grounding electrodes. The specific calculation methods are shown in Equations (4) and (5) [33]:

$$U_s = (1500 + 6\rho_s C_s)\frac{0.116}{\sqrt{t}} = \frac{174 + 0.7\rho_s C_s}{\sqrt{t}} \quad (4)$$

$$C_s = 1 - \frac{0.09\left(1 - \frac{\rho}{\rho_s}\right)}{2h_s + 0.09} \quad (5)$$

where U_s is the amplitude of the step voltage, C_s the surface soil attenuation factor, t the duration of the fault current, h_s the thickness of the surface layer, and ρ the resistivity of the underlying soil. Although existing theoretical calculation methods can provide calculations for the amplitude of the step voltage of grounding electrodes under power frequency conditions, they fail to adequately reflect the changes in the amplitude of the surface step voltage of grounding electrodes of different shapes under the influence of lightning strikes, as well as the distribution characteristics of the surface step voltage. Therefore, it is necessary to use simulation methods to compare and analyze the amplitude and distribution patterns of the surface step voltage of the grounding electrodes of different shapes.

3. SIMULATION METHODS AND THEORIES

The RESAP, HIFREQ, and FFTSES modules in the CDEGS electromagnetic analysis software package were used to evaluate the lightning protection capability of the transmission line grounding electrodes. The RESAP module was employed to model the soil conditions surrounding the transmission-line grounding electrodes, thereby supporting the construction of horizontally stratified soil models. Given that the focus of this study is on the quantitative comparison of the lightning protection capabilities of different-shaped radial grounding electrodes in transmission lines, the soil model was simplified to enhance the computational efficiency. A two-layer horizontal uniform soil model was selected, and soil conditions were simulated by altering the resistivity of the upper layer of the soil. The HIFREQ module was used to establish simulation models of different-shaped radial grounding electrodes, setting parameters such as the diameter, length, material type of the grounding material, amplitude of the power frequency injection current, current injection location, and burial depth. The FFTSES module was employed for the mathematical modeling of lightning currents and a fast Fourier transform. Specifically, the forward Fourier transform is used to input lightning current models with different parameters, whereas the inverse Fourier transform is utilized to convert the frequency-domain analysis data into time-domain data. A brief description of the calculation process and methods is shown in Figure 1 [34].

The simulation calculations mainly involve the theory of fast Fourier transform, which is used for the conversion between time-domain and frequency-domain lightning currents, as shown in Equations (6) to (9) [35, 36].

$$V(t) = \frac{1}{2\pi}\int_{-\infty}^{+\infty} V(\omega)e^{i\omega t}d\omega = \frac{1}{2\pi}\int_{-\infty}^{+\infty} V_0(\omega)I(\omega)e^{i\omega t}d\omega \quad (6)$$

$$E(t) = \frac{1}{2\pi}\int_{-\infty}^{+\infty} E(\omega)e^{i\omega t}d\omega = \frac{1}{2\pi}\int_{-\infty}^{+\infty} E_0(\omega)I(\omega)e^{i\omega t}d\omega \quad (7)$$

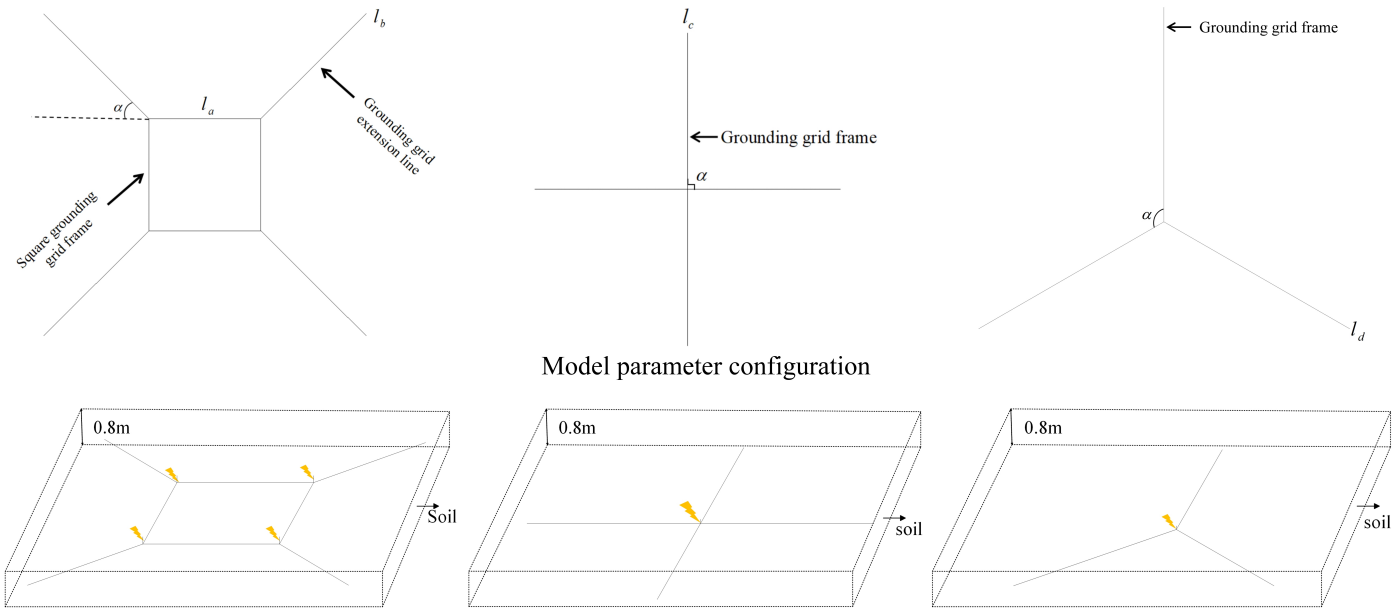

FIGURE 2. Grounding electrode simulation models.

$$H(t)=\frac{1}{2\pi}\int_{-\infty}^{+\infty}H(\omega)e^{i\omega t}d\omega=\frac{1}{2\pi}\int_{-\infty}^{+\infty}H_0(\omega)I(\omega)e^{i\omega t}d\omega \quad (8)$$

$$I(\omega)=\int_{-\infty}^{+\infty}I\,(t)e^{-j\omega t}dt \quad (9)$$

where ω represents the angular frequency, $V(t)$ the scalar potential generated by the lightning current in the time domain, $E(t)$ the electric field strength, and $H(t)$ the magnetic field strength. In the HIFREQ module, the frequencies produced by conductors after the application of lightning current mechanisms are typically represented by the unmodulated scalar potential, electric field strength, and magnetic field strength at the observation points and lines, which are defined as $V_0(\omega)$, $E_0(\omega)$, and $H_0(\omega)$, respectively. Unmodulated electromagnetic fields are generated by the excitation of the unit current applied to the conductor network. The frequency domain responses $V_0(\omega)$, $E_0(\omega)$, and $H_0(\omega)$ are calculated by HIFREQ, whereas the forward and inverse Fourier transforms are completed by FFTSES. In the software, the data must first be input into the working unit mode, specifying the path in the working directory. In HIFREQ, SESCAD is used for drawing and modeling, and the relevant parameters are set according to the research requirements in the soil type definition, followed by saving and running the data. For the calculation definition of the FFTSES module, inverse Fourier data calculations were performed. The maximum ground potential rise of the conductor segments and leakage current distribution of the grounding electrodes can be calculated using the corresponding conductor numbers. The impulse grounding resistance of the grounding electrodes was obtained by dividing the GPR of the conductor segments by the amplitude of the injected lightning current.

4. SIMULATION MODELS AND PARAMETER SETTINGS

4.1. Grounding Electrode Models

In this study, the CDEGS grounding simulation software was employed to construct simulation models of Y-shaped, cross-shaped, and rectangular ray-shaped grounding electrodes. Under the impact of high-frequency lightning currents, the grounding electrodes generate a significant impulse grounding inductance. The excessive extension of the horizontal rays of grounding electrodes can limit the reduction in their impulse grounding resistance, thereby affecting their lightning protection performance [37]. Therefore, to ensure consistency and validity of the models, the total length of the conductor material for grounding electrodes of different shapes was uniformly set to 100 m in this study. The established grounding electrode model is illustrated in Figure 2.

In the models, for the rectangular ray-shaped grounding electrode, the length of each conductor in the central square mesh frame was set to $l_a = 10$ m, the length of the external lead-out rays set to $l_b = 15$ m, and the angle between the extended lines of the single conductors in the square mesh area and the external lead-out rays set to $\alpha = 45°$. For the cross-shaped grounding electrode, the length of each single ray conductor was set to $l_c = 25$ m, and the angle between the rays was set to $\alpha = 90°$. For the Y-shaped grounding electrode, the length of each single ray conductor was set to $l_d = 33.5$ m, and the angle between the rays was set to $\alpha = 120°$. When the transmission line is struck by lightning, the lightning current dissipates into the soil through the four vertices of the rectangular ray-shaped grounding electrode and the center points of the Y- and cross-shaped grounding electrodes, as indicated by the lightning symbols in Figure 2. The burial depth of the grounding electrodes was uni-

formly set to 0.8 m; the conductor material uniformly was set to galvanized round steel with a relative resistivity of 10 Ω · m and a relative permeability of 300 H/m (compared with pure copper materials); and the radius of the conductors uniformly was set to 0.01 m.

4.2. Soil Model

In this study, the RESAP module of the CDEGS simulation software was used for soil modeling using the stratification method, as shown in Figure 3.

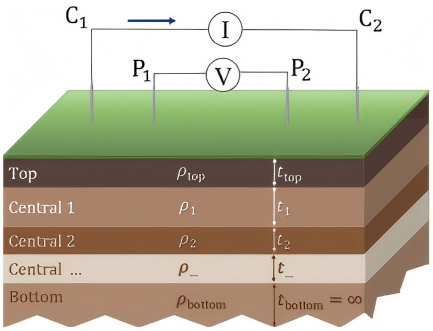

FIGURE 3. Stratification method of soil model.

To simplify the analysis, this study assumes that the entire grounding system is located on the same plane and that the soil resistivity is uniformly distributed. A horizontally uniform soil model was used, and different soil conditions were simulated by adjusting the soil resistivity parameter of the upper layer. To compare the impulse characteristics of different-shaped radial grounding electrodes under different soil resistivity conditions, the soil resistivity was set to 50 Ω · m, 150 Ω · m, 250 Ω · m, 350 Ω · m, 450 Ω · m, 550 Ω · m, 800 Ω · m, 1000 Ω · m, 1200 Ω · m, 1500 Ω · m, and 2000 Ω · m. (Among them, soil resistivities of 50 Ω · m and 150 Ω · m typically correspond to clay, 250 Ω · m to loess, 350 Ω · m and 450 Ω · m to stony soil, 600 Ω · m and 800 Ω · m to a mixture of gravel and soil, 1000 Ω · m to sand and gravel, and 2000 Ω · m to crushed stone). This study primarily focused on the influence of soil resistivity variations on the lightning transient characteristics of grounding electrodes. In soil modeling, a controlled-variable approach was adopted, where the relative dielectric constant of the soil was set to 1 and remained fixed, while simulations were conducted by varying the soil resistivity to obtain the results.

4.3. Lightning Current Model

In the simulation design, it was assumed that the entire grounding system was located on the same plane and that the soil resistivity was uniformly distributed. To compare the impulse characteristics of the three types of radial grounding electrodes under different soil resistivity conditions, the lightning current amplitude was set to 10 kA.

This study primarily investigated the influence of the shape of grounding electrodes on lightning transient characteristics under different soil resistivity conditions while maintaining the amplitude of the lightning current constant. The lightning current waveforms were set to 0.25/100 µs, 2.6/50 µs, 8/25 µs, and 10/350 µs. The sampling index was uniformly set to 2^{12}; the lightning current duration was selected under the complete waveform; and the maximum number of samples required to calculate the frequency response was uniformly set to 30. The input lightning current model is shown in Figure 4.

5. SIMULATION RESULTS AND DISCUSSION

5.1. Comparison of Grounding Resistance

Using the CDEGS HIFREQ module to input different soil and lightning current models for the numerical simulation, the power-frequency grounding resistance and impulse grounding resistance of the three types of grounding electrodes were obtained under soil resistivities of 50 Ω · m, 150 Ω · m, 250 Ω · m, 350 Ω · m, 450 Ω · m, 550 Ω · m, 800 Ω · m, 100 Ω · m, 120 Ω · m, 150 Ω · m, and 2000 Ω · m, respectively. The simulation results for the power frequency grounding resistance are shown in Figure 5, and the simulation results for the impulse grounding resistance are shown in Figure 6.

According to the simulation data shown in Figure 5, it can be observed that the power frequency grounding resistance of the rectangular ray-, Y-, and cross-shaped grounding electrodes increases approximately linearly with the increase in soil resistivity. Specifically, within the soil resistivity range of 50 Ω · m to 2000 Ω · m, under the same soil resistivity conditions, the power frequency grounding resistance of the rectangular ray-shaped grounding electrode was slightly higher than that of the cross-shaped grounding electrode with the same perimeter, and the power-frequency grounding resistance of the cross-shaped grounding electrode was slightly higher than that of the Y-shaped grounding electrode with the same perimeter. Moreover, the differences in power frequency grounding resistance among grounding electrodes of different shapes are not significant at low soil resistivities. However, as the soil resistivity increases, the differences in power frequency grounding resistance among grounding electrodes of different shapes also increase.

The simulation results shown in Figure 6 indicate that when the grounding electrodes are subjected to lightning currents with the same amplitude but different waveforms, the shorter the front time of the lightning current, the larger is the calculated impulse grounding resistance. Specifically, under the impact of a 0.25/100 µs waveform lightning current, the calculated impulse grounding resistance of the grounding electrodes was generally higher. For instance, the impulse grounding resistance of the rectangular ray-shaped grounding electrode is 76 Ω, while those of the Y-shaped and cross-shaped grounding electrodes are 73 Ω and 60.6 Ω, respectively. In contrast, under the 2.6/50 µs, 8/25 µs, and 10/350 µs waveforms, the impulse grounding resistances of the grounding electrodes of different shapes are closer to each other and are generally lower than those under the 0.25/100 µs waveform, with rectangular ray-shaped, Y-shaped, and cross-shaped grounding electrodes with impulse grounding resistances of approximately 49 Ω, 43 Ω, and 45 Ω, respectively.

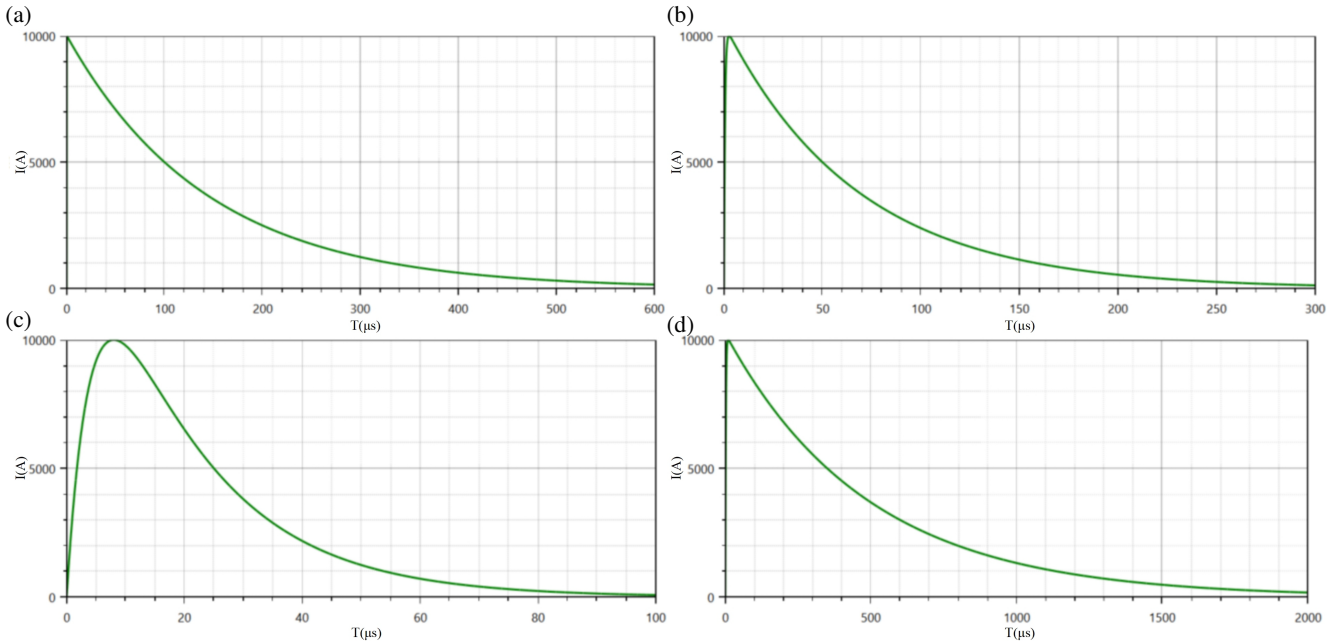

FIGURE 4. Input lightning current waveforms. (a) 0.25/100 μs waveform; (b) 2.6/50 μs waveform; (c) 8/25 μs waveform; (d) 10/350 μs waveform.

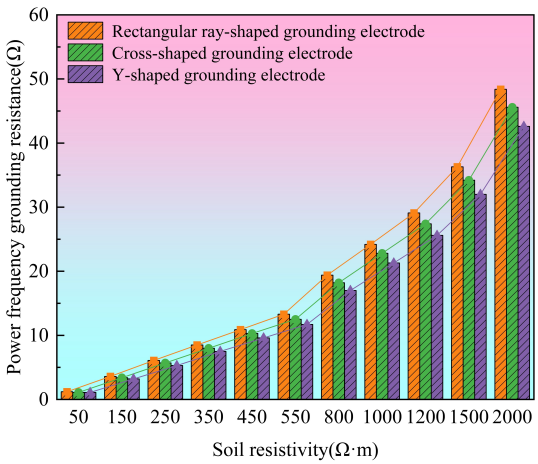

FIGURE 5. Power-frequency grounding resistance of the rectangular ray-shaped, cross-shaped, and Y-shaped electrodes under different soil resistivities.

These findings suggest that the effect of the lightning current waveform on the impulse grounding resistance of grounding electrodes becomes more pronounced with the shortening of the rise time and gradually weakens with the increase in the front time, with the differences in impulse grounding resistance among grounding electrodes of different shapes also decreasing. Further analysis shows that when the amplitude of the lightning current is fixed, the lightning current with a shorter rise time contains richer high-frequency components, leading to a decrease in the soil dielectric constant and electric-field gradient. Because the input amplitude of the lightning current was relatively small, the effect of soil ionization on the increase in the equivalent radius of the grounding electrode was limited. Therefore, in this study, the impulse potential distribution of the grounding electrodes is primarily affected by the inductive effect.

In summary, when the soil resistivity is below 150 Ω · m, a rectangular ray-shaped grounding electrode is recommended for installation because of its smaller land occupation, power frequency grounding resistance comparable to the other two shapes, and lower impulse grounding resistance under different lightning current waveforms. When the soil resistivity was high, the cross- and Y-shaped grounding electrodes demonstrated superior performance. Specifically, in mountainous areas with a high lightning density or rugged roads, a cross-shaped grounding electrode is recommended because of its smaller land occupation and lower inductive effect. In areas with high soil resistivity and infrequent lightning phenomena, the Y-shaped grounding electrode should be prioritized for installation because of its overall better lightning protection performance.

5.2. Comparison of Ground Potential Rise

As analyzed in Section 5.1, there is a significant difference in the impulse characteristics of grounding electrodes in areas with low soil resistivity (less than 150 Ω · m) and areas with high soil resistivity. To quantitatively analyze and compare the distribution patterns of the ground potential rise for grounding electrodes of different shapes, the simulation model was set based on the impulse grounding resistance data of different grounding electrodes, as shown in Figure 6. Two soil resistivity conditions (150 Ω · m and 2000 Ω · m) were established, with the burial depth of the grounding electrodes uniformly set to 0.8 m. The lightning current waveforms were set to 0.25/100 μs, 2.6/50 μs, 8/25 μs, and 10/350 μs, and the amplitude of the lightning current was uniformly set to 10 kA. Under these conditions, the three-dimensional distribution and

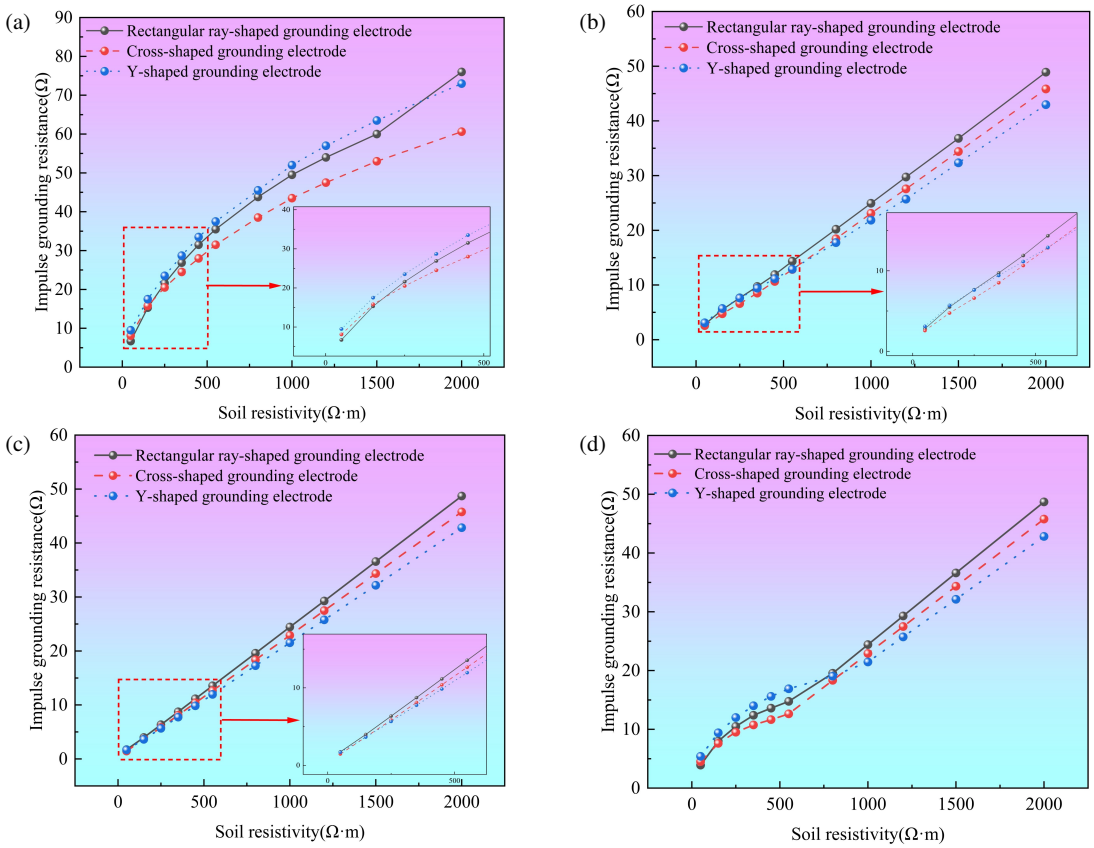

FIGURE 6. Impulse grounding resistance of the rectangular ray-shaped, cross-shaped, and Y-shaped grounding electrodes under different lightning current waveforms: (a) 0.25/100 μs; (b) 2.6/50 μs; (c) 8/25 μs; (d) 10/350 μs.

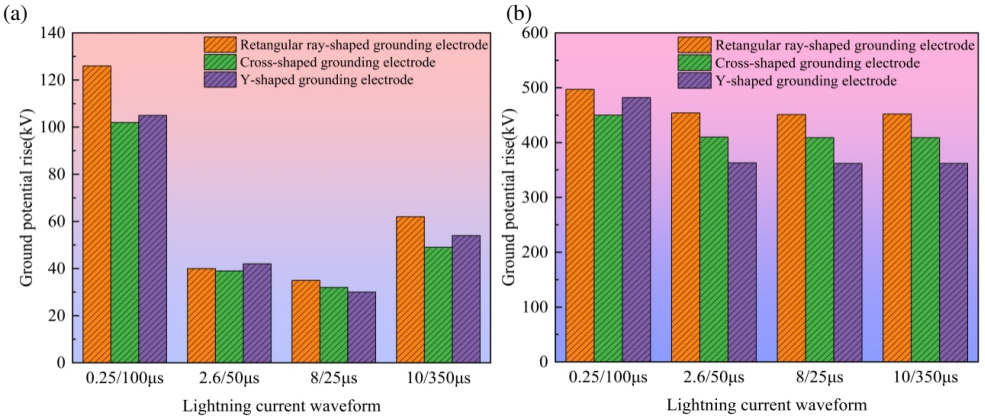

FIGURE 7. Maximum amplitude: (a) 150 Ω · m; (b) 2000 Ω · m.

maximum amplitude simulation results of the ground potential rise for grounding electrodes of different shapes are shown in Figures 7 to 9, respectively.

The simulation results in Figures 7 to 9 reveal the impact of lightning current waveforms on the ground potential rise of grounding electrodes under different soil resistivities. When the amplitude of the lightning current was the same, in areas with low soil resistivity (150 Ω · m), changes in the lightning current waveform significantly affected the maximum amplitude and three-dimensional distribution pattern of the ground potential rise. In contrast, in areas with high soil resistivity (2000 Ω · m), the impact of changes in the lightning current waveform on the maximum amplitude and three-dimensional distribution pattern of the ground potential rise is relatively small. Specifically, in areas with a soil resistivity of 150 Ω · m, under the 0.25/100 μs and 8/25 μs waveforms, the maximum amplitude of the ground potential rise of the grounding electrodes was significantly higher than those of the other two waveforms. The three-dimensional distribution shows a more concentrated area of increased ground potential rise, and the differences in the amplitude of the ground potential rise under different waveforms are more pronounced.

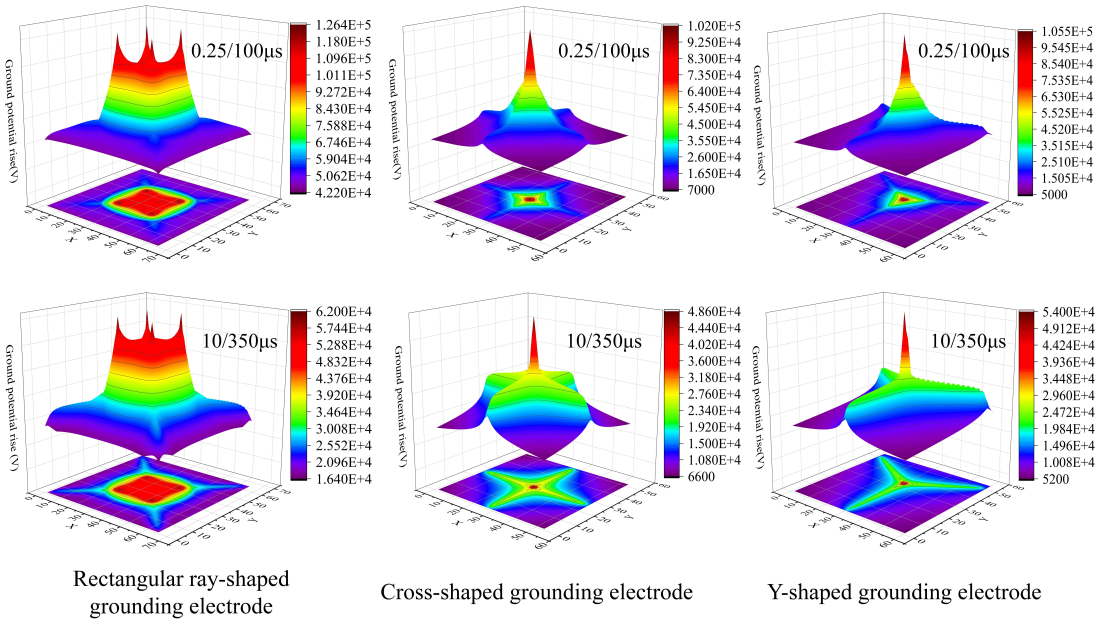

FIGURE 8. Three-dimensional distribution of ground potential rise for grounding electrodes at soil resistivity of 150 Ω · m. The 3D and contour plots show that in low-resistivity soil, the magnitude and spatial distribution of the potential rise are strongly influenced by the waveform of the lightning current.

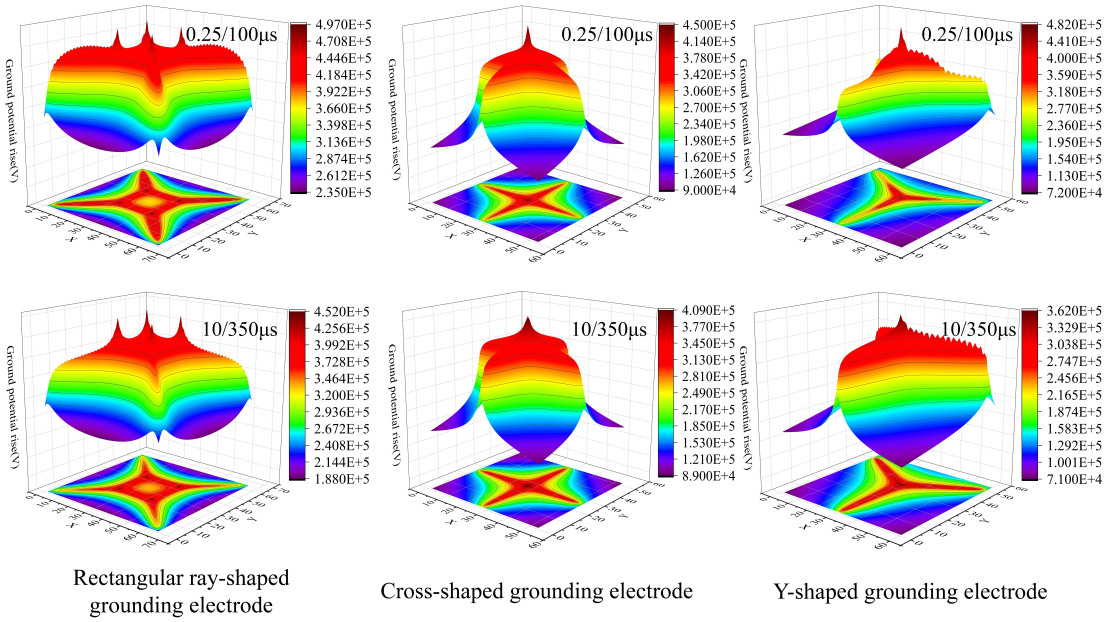

FIGURE 9. Three-dimensional distribution of ground potential rise for grounding electrodes at soil resistivity of 2000 Ω · m. The results indicate that in high-resistivity soil, the spatial patterns under different waveforms become more uniform, although the rectangular ray-shaped electrode exhibits higher peak values.

A comparative analysis of the distribution patterns of ground potential rise for grounding electrodes of different shapes reveals that in areas with low soil resistivity (150 Ω · m), under the 0.25/100 μs and 10/350 μs lightning current waveforms, the rectangular ray-shaped grounding electrode has a larger area of ground potential distribution around the injection point, mainly concentrated in the central square mesh area and decreasing layer by layer towards the periphery along the external lead-out rays. In contrast, the cross-shaped and Y-shaped grounding electrodes have a smaller area of ground potential distribution around the injection point, presenting a pattern that converges to a sharp end and decreases layer-by-layer towards the far end in a square and triangular ring distribution, respectively. Under the 2.6/50 μs and 8/25 μs lightning current waveforms, the characteristics of the ground potential distribution along the external lead-out rays of the grounding electrodes of different shapes become more pronounced. In particular, under the 8/25 μs lightning current waveform, the grounding electrode had the largest area of ground potential distribution.

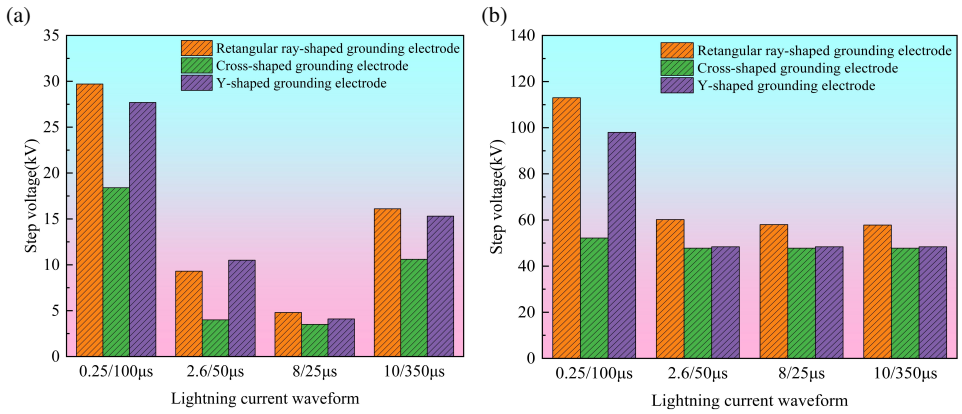

FIGURE 10. Maximum amplitude: (a) 150 Ω · m; (b) 2000 Ω · m.

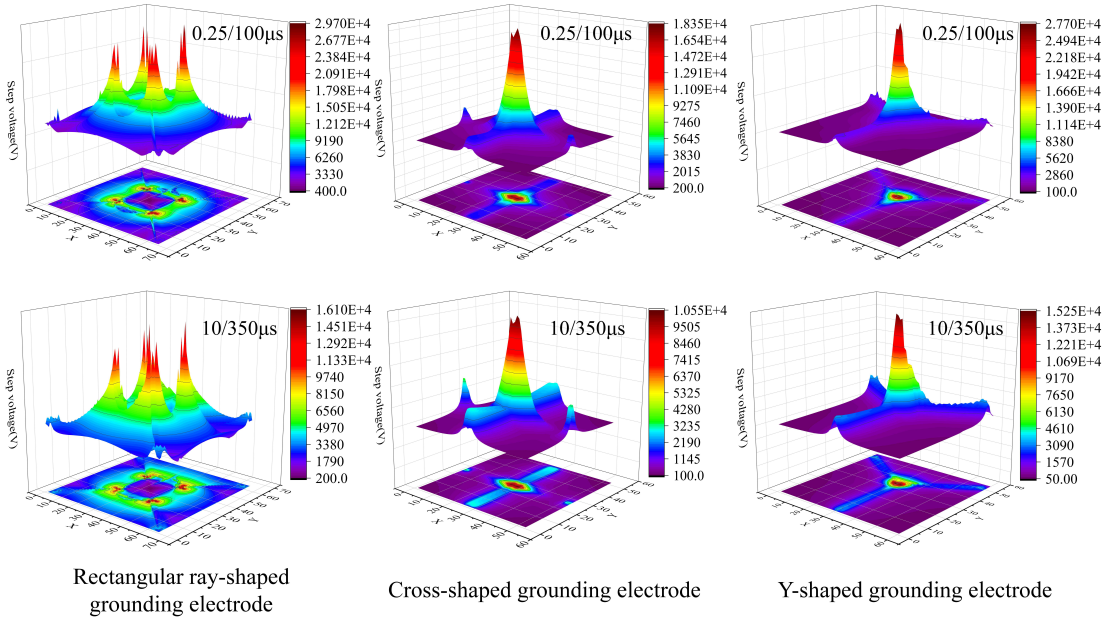

FIGURE 11. Three-dimensional distribution of step voltage for grounding electrodes at soil resistivity of 150 Ω · m.

In areas with high soil resistivity (2000 Ω · m), the distribution patterns of the ground potential for grounding electrodes under different lightning current waveforms tended to be consistent, showing a pattern of outward diffusion along the extended rays from the lightning current injection point, with roughly the same area of ground potential distribution. In areas with a soil resistivity of 2000 Ω · m, the rectangular ray-shaped grounding electrode had a significantly higher maximum amplitude of ground potential rise under different lightning current waveforms than the other two grounding electrode shapes. The three-dimensional distribution results show that the ground potential rise amplitude distribution parameters are generally greater than those of the Y-shaped and cross-shaped grounding electrodes. These results further support the view that cross- and Y-shaped grounding electrodes should be preferred in areas with high soil resistivity.

5.3. Comparison of Step Voltage

The soil resistivity was set to 150 Ω · m and 2000 Ω · m; the burial depth of the grounding electrodes was uniformly set to 0.8 m; the lightning current waveforms were set to 0.25/100 μs, 2.6/50 μs, 8/25 μs, and 10/350 μs; and the amplitude of the lightning current was uniformly set to 10 kA. Under these conditions, the three-dimensional distribution and maximum amplitude simulation results of the step voltage for grounding electrodes of different shapes are shown in Figures 10 and 12, respectively.

The simulation results (as shown in Figures 10–12) indicate that the waveform of the lightning current significantly affects the step voltage of the grounding electrodes under different soil resistivities. When the amplitude of the lightning current is the same, in areas with low soil resistivity (150 Ω · m), changes in the waveform of the lightning current have a significant impact on the maximum amplitude and the three-dimensional distribution pattern of the step voltage. In contrast, in areas with high soil resistivity (2000 Ω · m), this impact was relatively small. Specifically, under the soil resistivity condition of 150 Ω · m, the maximum amplitude of the step voltage of the grounding electrodes under the 0.25/100 μs and 8/25 μs waveforms was significantly higher than that of the other two waveforms. In the

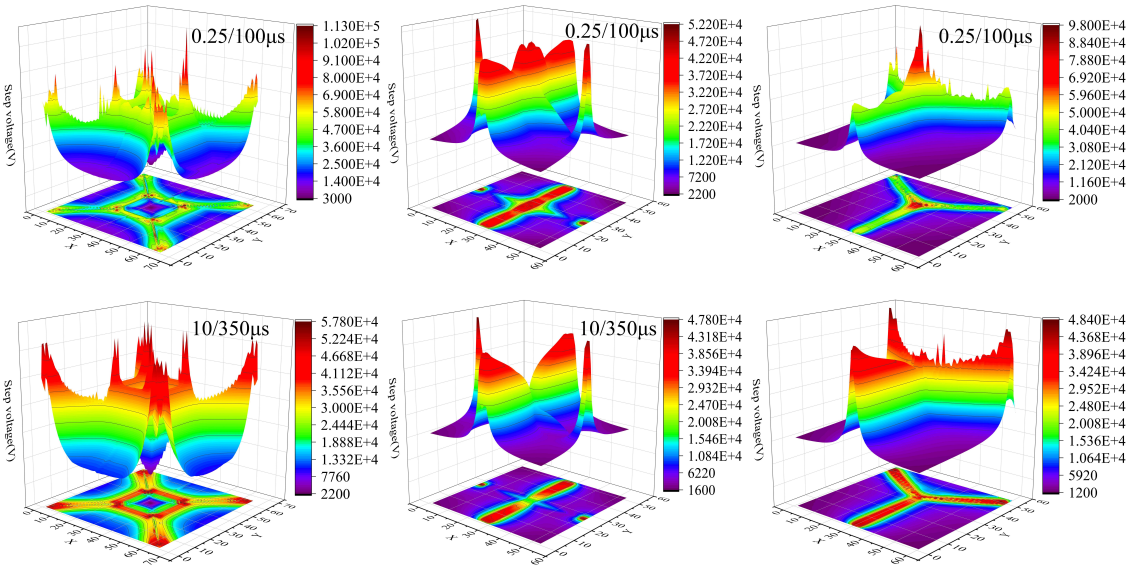

FIGURE 12. Three-dimensional distribution of step voltage for grounding electrodes at soil resistivity of 2000 Ω · m.

three-dimensional distribution, the high-amplitude areas of the step voltage were mainly concentrated around the lightning current injection points, with no obvious distribution trend along the external lead-out rays. The differences in the maximum amplitude of the step voltage for different waveforms were more pronounced. Under the soil resistivity condition of 2000 Ω · m, the maximum amplitude of the step voltage of the grounding electrodes under the 0.25/100 μs lightning current waveform was significantly higher than those under the other three waveforms.

A comparative analysis of the distribution patterns of step voltage for grounding electrodes of different shapes reveals that in areas with low soil resistivity (150 Ω · m), under the 0.25/100 μs and 10/350 μs lightning current waveforms, the rectangular ray-shaped grounding electrode has a larger area of step voltage distribution around the injection point, mainly distributed along the square mesh frame, whereas the distribution along the external lead-out rays is not obvious. The high-amplitude step voltage of the cross- and Y-shaped grounding electrodes is mainly distributed around the current injection point, presenting a ring-shaped distribution pattern, with no obvious step voltage distribution along the external lead-out rays.

Under the 2.6/50 μs and 10/350 μs lightning current waveforms, the distribution trend of the step voltage along the external lead-out rays of the grounding electrodes became more pronounced. The high-amplitude area of the step voltage for the rectangular ray-shaped grounding electrode is mainly distributed along the square mesh frame and the external lead-out rays, whereas the high-amplitude area of the step voltage for the cross-shaped and Y-shaped grounding electrodes is mainly distributed along the external lead-out rays. In areas with high soil resistivity (2000 Ω · m), under the 0.25/100 μs lightning current waveform, the high-amplitude area of the step voltage for the grounding electrodes was mainly distributed around the current injection point, with a tendency to diffuse along the external lead-out rays, but the distribution area of the high-amplitude area was relatively small. Under the 2.6/50 μs, 8/25 μs, and 10/350 μs lightning current waveforms, the distribution area of the high-amplitude area of the step voltage for the grounding electrodes on the external lead-out rays increased significantly, presenting a distribution characteristic different from that under the 0.25/100 μs lightning current waveform.

In areas with high soil resistivity (2000 Ω · m), the maximum amplitude of the step voltage of the rectangular ray-shaped grounding electrode under different lightning current waveforms was significantly higher than those of the other two grounding electrode shapes. The three-dimensional distribution results show that the step voltage distribution parameters of the rectangular ray-shaped grounding electrode are greater than those of the cross- and Y-shaped grounding electrodes. The above results further support the view that cross-shaped and Y-shaped grounding electrodes are preferred in areas with high soil resistivity, and cross-shaped grounding electrodes are preferred in areas with high lightning density.

5.4. Comparison of Spectral Response Characteristics

The amplitude of the injected lightning current was set to 100 kA, and the soil resistivity was set to 150 Ω · m and 2000 Ω · m. The burial depth of the grounding electrodes was set to 0.8 m. The frequency parameter coverage ranged widely from 1 Hz to 100000 kHz, specifically, 1 Hz, 5 Hz, 10 Hz, 50 Hz, 100 Hz, 1 kHz, 5 kHz, 10 kHz, 100 kHz, 1000 kHz, and 10000 kHz. Under these conditions, the frequency-domain response results of the grounding impedance values and grounding impedance angles for grounding electrodes of different shapes are shown in Figure 13.

From the simulation results shown in Figure 13, a comparison of the frequency domain response of the grounding impedance values for grounding electrodes under different soil

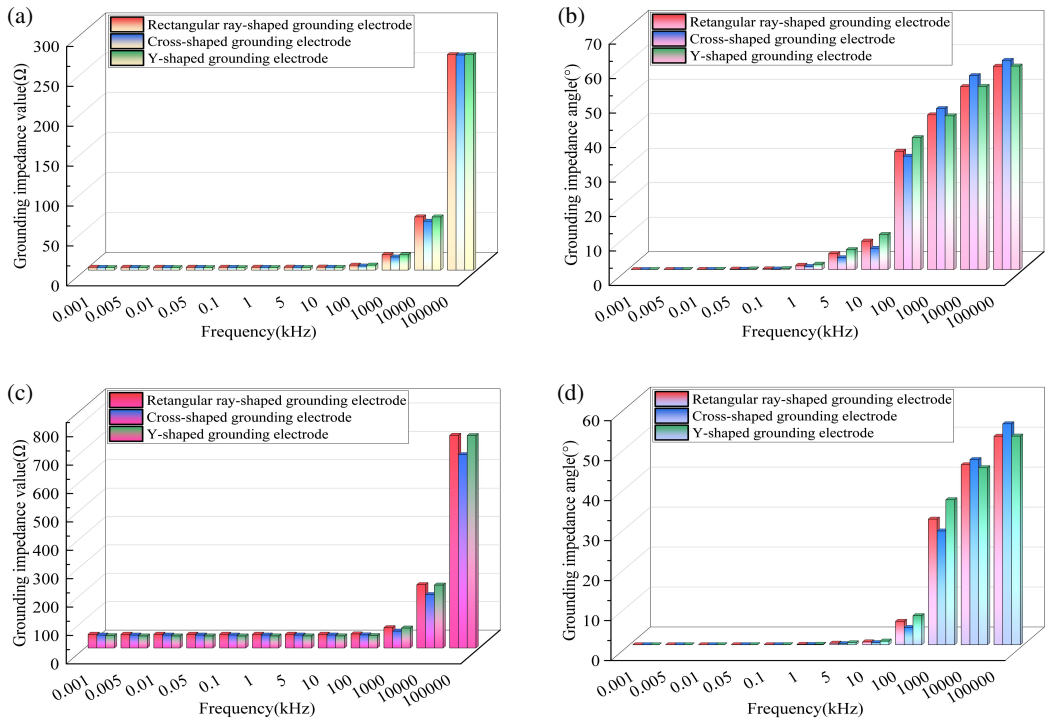

FIGURE 13. Frequency-domain responses of grounding impedance magnitude and phase angle for the grounding electrode under different soil resistivities: (a) and (b) 150 Ω · m; (c) and (d) 2000 Ω · m.

resistivities reveals that an increase in soil resistivity leads to a significant increase in the grounding impedance values. In areas with low soil resistivity (150 Ω · m), when the frequency is below 100 kHz, the grounding impedance values of the three types of grounding electrodes are essentially independent of the frequency changes and are relatively close to each other. When the frequency is in the range of 100 kHz to 10000 kHz, the grounding impedance values of the rectangular ray- and Y-shaped grounding electrodes are slightly higher than those of the cross-shaped grounding electrode. At a frequency of 100000 kHz, the grounding impedance values of the three types of grounding electrodes tend to converge. In areas with high soil resistivity (2000 Ω · m), the grounding impedance values of the rectangular ray-shaped grounding electrode were slightly higher than those of the cross- and Y-shaped grounding electrodes at different frequencies. When the frequency was less than 100 kHz, the grounding impedance values of the cross-shaped and Y-shaped grounding electrodes were relatively close. However, when the frequency exceeds 100 kHz, the grounding impedance values of the rectangular ray-shaped and Y-shaped grounding electrodes were significantly higher than those of the cross-shaped grounding electrode, indicating that high-frequency lightning currents had a lesser impact on the lightning protection performance of the cross-shaped grounding electrode.

A comparison of the frequency domain response of the grounding impedance angles for grounding electrodes under different soil resistivities reveals that the grounding impedance angle is less affected by changes in soil resistivity and is more significantly influenced by frequency variations. In areas with low soil resistivity (150 Ω · m), when the frequency was below 1 kHz, the grounding impedance angles of the three types of grounding electrodes were relatively close and all below 10°. When the frequency is in the range of 1 kHz–100 kHz, the Y-shaped grounding electrode has the largest grounding impedance angle. When the frequency exceeds 100 kHz, the rectangular ray-shaped grounding electrode exhibited the largest grounding impedance angle. In areas with high soil resistivity (2000 Ω · m), the differences in the grounding impedance angles among grounding electrodes of different shapes become more pronounced at frequencies above 100 kHz. These results further support the view that cross- and Y-shaped grounding electrodes should be preferred in areas with high soil resistivity, and cross-shaped grounding electrodes should be prioritized in areas with high lightning density.

6. CONCLUSION

This study quantitatively compared the impulse dissipation characteristics of radial grounding electrodes with different shapes under lightning strike conditions and reached the following conclusions.

a) Under low soil resistivity conditions, the differences in the power frequency grounding resistance among the grounding electrodes of different shapes are relatively small, and these differences gradually increase with the increase in soil resistivity. The effect of the lightning current waveform on the impulse grounding resistance is significantly enhanced by shortening the rise time of the waveform. Under the 0.25/100 µs waveform, the impulse grounding re-

sistance of the cross-shaped grounding electrode is sinificantly lower than that of the Y-shaped grounding electrode. However, under other waveforms, the impulse grounding resistance of the Y-shaped grounding electrode is relatively lower, indicating that under high-energy lightning current impacts, the Y-shaped grounding electrode exhibits a more pronounced inductive effect compared to the cross-shaped grounding electrode.

b) Under soil resistivity conditions of $150\,\Omega\cdot$m, the maximum amplitude of the ground potential rise of the rectangular ray-shaped grounding electrode was similar tothat of the other two grounding electrode shapes. Under high soil resistivity conditions of $2000\,\Omega\cdot$m, its value was significantly higher than that of the cross-shaped and Y-shaped grounding electrodes.

c) In areas with low soil resistivity ($150\,\Omega\cdot$m), when the amplitude of the lightning current is the same, changes in the waveform of the lightning current significantly affect the maximum amplitude and three-dimensional distribution pattern of the step voltage for the radial grounding electrodes. In areas with high soil resistivity ($2000\,\Omega\cdot$m), the distribution patterns of the step voltage for the grounding electrodes of different shapes were more similar in the three-dimensional distribution. Under different lightning current waveforms, the maximum amplitude of the step voltage of the rectangular ray-shaped grounding electrode was significantly higher than that of the cross- and Y-shaped grounding electrodes.

d) An increase in soil resistivity significantly increases the grounding impedance values of the radial grounding electrodes. In areas with high soil resistivity ($2000\,\Omega\cdot$m), the grounding impedance values of the rectangular ray-shaped grounding electrode were generally higher than those of the cross- and Y-shaped grounding electrodes at different frequencies. The grounding impedance angle was less affected by changes in soil resistivity and was more significantly influenced by frequency variations. In areas with high soil resistivity ($2000\,\Omega\cdot$m), the differences in the grounding impedance angles among the grounding electrodes of different shapes become more pronounced at frequencies above 100 kHz.

In summary, in areas with low soil resistivity (approximately $150\,\Omega\cdot$m), selecting a rectangular ray-shaped grounding electrode as the grounding electrode for transmission line towers offers better impulse characteristics and dissipation effects. In areas with high soil resistivity (approximately $2000\,\Omega\cdot$m), choosing cross-shaped and Y-shaped grounding electrodes as the grounding electrodes for transmission line towers provides superior impulse characteristics and dissipation effects. In this study, the lightning transient characteristics of grounding electrodes with different shapes were investigated under a lightning current amplitude of 10 kA. The CDEGS simulation software could not adequately reflect the nonlinear soil effects caused by the spark effect. Future work could conduct studies under different lightning current amplitudes and fully consider the spark effect and soil nonlinearity.

ACKNOWLEDGEMENT

This study was supported financially by the Key Research and Development Program of Shaanxi (No. 2024GX-YBXM-519).

REFERENCES

[1] Wu, H., J. Wang, D. Nan, Q. Cui, and W. Li, "Fault location and fault cause identification method for transmission lines based on pose normalized multi-output convolutional nets," *IEEE Transactions on Instrumentation and Measurement*, Vol. 74, 1–12, 2025.

[2] Guo, J., Q.-S. Zheng, W.-C. Xie, Y.-Z. Xie, and S. V. Tkachenko, "High-frequency electromagnetic field coupling to transmission line with discontinuity above a lossy ground," *IEEE Transactions on Electromagnetic Compatibility*, Vol. 66, No. 2, 615–625, Apr. 2024.

[3] Bourscheidt, V., O. Pinto, and K. P. Naccarato, "Improvements on lightning density estimation based on analysis of lightning location system performance parameters: Brazilian case," *IEEE Transactions on Geoscience and Remote Sensing*, Vol. 52, No. 3, 1648–1657, Mar. 2014.

[4] Nasir, N. A. F. M., M. Z. A. A. Kadir, M. Osman, M. S. A. Rahman, U. A. U. Amirulddin, M. S. M. Nasir, N. H. Zaini, and N. H. N. Ali, "Impact of earthing system designs and soil characteristics on tower footing impedance and ground potential rise: A modelling approach for sustainable power operation," *Sustainability*, Vol. 13, No. 15, 8370, Jul. 2021.

[5] Hu, Y., Y. Cheng, Z. Jiang, Y. An, S. Jeon, and W. Zhou, "Simulation and structure optimization of grounding circuit model for power transmission line tower," *Journal of Circuits, Systems and Computers*, Vol. 31, No. 16, 2250278, 2022.

[6] Formisano, A., S. Barmada, and M. Raugi, "Impact of nearby lightning strikes on wireless power transfer ground assembly," *IEEE Transactions on Magnetics*, Vol. 59, No. 5, 1–4, May 2023.

[7] Heidler, F. H. and C. Paul, "Field enhancement by lightning strikes to tall tower versus lightning strikes to flat ground," *IEEE Transactions on Electromagnetic Compatibility*, Vol. 63, No. 2, 550–557, Apr. 2021.

[8] Koike, S., Y. Baba, T. Tsuboi, and V. A. Rakov, "Lightning current waveforms inferred from far-field waveforms for the case of strikes to tall objects," *IEEE Transactions on Electromagnetic Compatibility*, Vol. 65, No. 4, 1162–1169, Aug. 2023.

[9] Ishimoto, K., F. Tossani, F. Napolitano, A. Borghetti, and C. A. Nucci, "Direct lightning performance of distribution lines with shield wire considering lemp effect," *IEEE Transactions on Power Delivery*, Vol. 37, No. 1, 76–84, Feb. 2022.

[10] Shariatinasab, R., J. G. Safar, J. Gholinezhad, and J. He, "Analysis of lightning-related stress in transmission lines considering ionization and frequency-dependent properties of the soil in grounding systems," *IEEE Transactions on Electromagnetic Compatibility*, Vol. 62, No. 6, 2849–2857, Dec. 2020.

[11] Datsios, Z. G., P. N. Mikropoulos, and T. E. Tsovilis, "Effects of lightning channel equivalent impedance on lightning performance of overhead transmission lines," *IEEE Transactions on Electromagnetic Compatibility*, Vol. 61, No. 3, 623–630, Jun. 2019.

[12] Paul, C., F. H. Heidler, and W. Schulz, "Performance of the european lightning detection network EUCLID in case of various types of current pulses from upward lightning measured at the Peissenberg Tower," *IEEE Transactions on Electromagnetic Compatibility*, Vol. 62, No. 1, 116–123, 2020.

[13] Velásquez, R. M. A. and J. V. M. Lara, "Failures in overhead lines grounding system and a new improve in the IEEE and national standards," *Engineering Failure Analysis*, Vol. 100, 103–118, 2019.

[14] Sekioka, S., H. Hayashida, T. Hara, and A. Ametani, "Measurements of grounding resistances for high impulse currents," *IEE Proceedings — Generation, Transmission and Distribution*, Vol. 145, No. 6, 693–699, Nov. 1998.

[15] Ramamoorty, M., M. M. B. Narayanan, S. Parameswaran, and D. Mukhedkar, "Transient performance of grounding grids," *IEEE Transactions on Power Delivery*, Vol. 4, No. 4, 2053–2059, Oct. 1989.

[16] Motoyama, H., "Electromagnetic transient response of buried bare wire and ground grid," *IEEE Transactions on Power Delivery*, Vol. 22, No. 3, 1673–1679, Jul. 2007.

[17] Motoyama, H., "Experimental and analytical studies on lightning surge characteristics of a buried bare wire," *Electrical Engineering in Japan*, Vol. 164, No. 3, 35–41, Aug. 2008.

[18] Visacro, S. and G. Rosado, "Response of grounding electrodes to impulsive currents: An experimental evaluation," *IEEE Transactions on Electromagnetic Compatibility*, Vol. 51, No. 1, 161–164, Feb. 2009.

[19] Bezerra, G. V. N., F. A. Moreira, T. V. Ferreira, and R. Alipio, "Concrete encased grounding: Lightning response analysis considering the frequency dependence of soil," *IEEE Transactions on Electromagnetic Compatibility*, Vol. 66, No. 3, 879–889, Jun. 2024.

[20] Kumar, A. S., P. K. Bhandiwad, and K. Manickavasagam, "Impulse efficient optimum impedance grounding electrode configuration for lightning transients," *IEEE Transactions on Electromagnetic Compatibility*, Vol. 65, No. 6, 1990–1997, Dec. 2023.

[21] Kumar A, S. and K. Manickavasagam, "Computation of effective length of enhancement for vertical electrode under lightning transients," *IEEE Transactions on Electromagnetic Compatibility*, Vol. 64, No. 6, 2141–2148, Dec. 2022.

[22] Clark, D., S. Mousa, N. Harid, H. Griffiths, and A. Haddad, "Lightning current performance of conventional and enhanced rod ground electrodes," *IEEE Transactions on Electromagnetic Compatibility*, Vol. 63, No. 4, 1179–1188, Aug. 2021.

[23] Grcev, L., B. Markovski, and M. Todorovski, "General formulas for lightning impulse impedance of horizontal and vertical grounding electrodes," *IEEE Transactions on Power Delivery*, Vol. 36, No. 4, 2245–2248, Aug. 2021.

[24] Grcev, L., B. Markovski, and M. Todorovski, "Lightning performance of multiple horizontal, vertical and inclined grounding electrodes," *IEEE Transactions on Power Delivery*, Vol. 37, No. 5, 3782–3791, Oct. 2022.

[25] Xue, J., H. Huang, L. Cai, Z. Xu, Y. Fang, J. Wang, and Y. Fan, "Lightning impulse impedance and surface potential distribution of 10 kV distribution line tower: Field test and simulation," *IEEE Transactions on Power Delivery*, Vol. 37, No. 1, 415–422, Feb. 2022.

[26] Huang, L., L. Zhou, D. Zhang, D. Wang, W. Gu, and S. Chen, "Research on impulse impedance model and protection optimization of transmission tower grounding device in mountainous area," *IET Science, Measurement & Technology*, Vol. 15, No. 8, 632–644, Oct. 2021.

[27] Dan, Y., R. Zhang, Y. Wu, Y. Li, X. Wang, and J. Yang, "Tower impulse grounding resistance measurement based on multiple frequency impedance," *IET Generation, Transmission & Distribution*, Vol. 17, No. 15, 3488–3500, Aug. 2023.

[28] Dan, Y., J. Yin, J. Yang, and H. Yang, "Influence analysis of calculated horizontally layered soil parameters on grounding parameters," *High Voltage*, Vol. 8, No. 2, 421–430, Apr. 2023.

[29] Gao, F., L. Yang, J. Guo, J. Zhang, J. Wang, and Y. Li, "Research on impulse characteristics and simulation model of single extended grounding electrode," *High Voltage Apparatus*, Vol. 56, No. 4, 148–152,158, 2020 (in Chinese).

[30] Qi, S. and H. Zhao, "Optimization and design of protection characteristics for radial grounding conductors of line towers," *Power System And Clean Energy*, Vol. 38, No. 1, 1–6, Jan. 2022.

[31] Shi, F., D. Yang, X. Wang, H. Song, T. Yang, and X. Hu, "Quantitative comparison of impact characteristics between circular grounding body and herringbone grounding body," *Insulators and Surge Arresters*, No. 6, 130–136, 158, Dec. 2022 (in Chinese).

[32] Liu, W., Y. Hu, H. Tian, Z. Jiang, X. Su, J. Xiong, W. Su, and Y. Wang, "Research on lightning overvoltage protection of line-adjacent pipelines based on solid-state decoupling," *Applied Sciences*, Vol. 13, No. 22, 12529, Nov. 2023.

[33] Alyami, S., "Grid grounding calculations for a 132-KV substation using soil backfilling," *IEEE Access*, Vol. 7, 104 933–104 940, Aug. 2019.

[34] Zhang, J., W. Cao, and S. Hu, "The influence of transmission corridor tower grounding electrode shapes on the impulse interference of adjacent secondary cables," *Advances in Electrical and Computer Engineering*, Vol. 25, No. 3, 3–12, 2025.

[35] Wang, X., Y. Wang, T. Sun, X. Yang, L. Yang, and Y. Qi, "Study of transmission line AC interference with steel-buried pipelines under lightning strikes," *Electric Power Systems Research*, Vol. 218, 109226, May 2023.

[36] Liu, Y., J. Wang, P. Zhao, Y. Tao, Z. Xu, X. Yan, and C. Xu, "Refined modeling calculation of electromagnetic fields when lightning strikes thermal power plant and optimized layouts of sensitive devices," *Electric Power Systems Research*, Vol. 202, 107562, Jan. 2022.

[37] Guo, L., W. Gu, B. Liu, Y. Zeng, and S. Chen, "Impulse impedance modeling and application of tower grounding device," *Transactions of China Electrotechnical Society*, Vol. 35, No. 10, 2239–2247, 2020.